# pH and ionic strength responsive core-shell protein microgels fabricated via simple coacervation of soy globulins

Nannan Chen, Taco Nicolaï, Christophe Chassenieux, Yong Wang

# pH and ionic strength responsive core-shell protein microgels fabricated via simple coacervation of soy globulins

Nannan Chen,[a] Taco Nicolai,[b] Christophe Chassenieux,[b] Yong Wang[a,*]

[a]*Guangdong Saskatchewan Oilseed Joint Laboratory, Department of Food Science and Engineering, Jinan University, Guangzhou 510632, China*

[b]*Le Mans Université, IMMM UMR-CNRS 6283, Polymères, Colloïdes et Interfaces, 72085 Le Mans cedex 9, France*

## Abstract

The influence of the salt concentration, pH, protein concentration and temperature was investigated on spontaneous reversible coacervation in soy protein isolate (SPI) solutions. Coacervation was characterized by formation of protein enriched micro-domains and was most significant at 0.1 M NaCl. It was predominant below 40 °C and favored by lowering the temperature. Decreasing the pH caused the spherical coacervates to form irregular flocs. Increasing the protein concentration led to the formation of larger coacervates, but lowered the rates of coacervation. Irreversibly crosslinked microgels were fabricated by heating suspensions of coacervates at 80 ºC. The effects of the pH and the salt concentration on the morphology and the protein composition of the microgels were analyzed. The microgels swelled and displayed a core-shell structure when the electrostatic repulsion between proteins was increased by removing salt or adjusting the pH away from the isoelectric point. Reducing the electrostatic repulsion induced de-swelling of the microgels and disappearance of the core-shell structure. By tuning the electrostatic interaction, the SPI microgels could bind or release positively charged lysozyme. These results show that SPI microgels are promising bioactive compound carriers.

**Keywords:** Soy protein isolate; coacervation; phase separation; microgel; swelling; release

## 1. Introduction

Microgels are microparticles consisting of a network of crosslinked macromolecules (Plamper & Richtering, 2017; Wang, Guo, Dong, Cui, & Hao, 2019). Due to their swelling and de-swelling behavior upon changes of the environmental conditions, they can be used to encapsulate bioactive compounds and control their release (Bysell, Mansson, Hansson, & Malmsten, 2011). They have also been used to modify the rheology properties of food matrices (Inthavong, Chassenieux, & Nicolai, 2019; Sağlam, Venema, de Vries, Shi, & van der Linden, 2013) and to stabilize emulsions and foams (Dickinson, 2015). Protein is one of the promising materials to fabricate microgels as it is biocompatible and environmental friendly. The swelling and de-swelling of protein gels can be modulated by the pH and the ionic strength, due to the presence of charged acidic (e.g. carboxylic) and basic (e.g. ammonium) groups in the polypeptide chains (Sağlam, Venema, de Vries, & van der Linden, 2013). Stable protein gels can be formed either by heating or by cold-gelation through hydrophobic interactions, disulfide bonds or hydrogen bonds without the need to add chemical crosslinkers (Chen, Remondetto, & Subirade, 2006).

Several approaches have been developed to fabricate protein microgels. Protein microgels with sizes of several hundred nanometers have been obtained by mechanical breakup of bulk protein gels (Jiao, Shi, Wang, & Binks, 2018; Murray & Phisarnchananan, 2016). Whey protein/β-lactoglobulin microgels with sizes around 200 nm have been fabricated by heating solutions in a narrow pH range close to the isoelectric point (Schmitt et al., 2010) or in the presence of $CaCl_2$ (Phan-Xuan et al., 2014). Creating micro-domains of a protein dense phase followed by heating is another efficient method to make whey protein microgels which can be

achieved with water in oil emulsions (Sağlam, Venema, de Vries, Sagis, & van der Linden, 2011) or by segregative phase separation in mixtures with polysaccharides (Aymard, Williams, Clark, & Norton, 2000). During heating, the dense protein domains crosslink into microgels with sizes larger than a micrometer. Much work has been done to fabricate milk protein based microgels, but fabrication of microgels based on plant proteins is much less common. Compared to animal protein, plant protein is more abundant and economical. There is currently an increasing effort to explore the possibility to replace animal proteins with plant proteins in food products, in view of the shortage of animal proteins for an increasing world population and the environmental problems caused by animal husbandry (Alves & Tavares, 2019).

Variation of the solvent conditions, such as temperature, pH and ionic strength can induce simple coacervation (self-coacervation) of protein in solution leading to liquid-liquid microphase separation (LLPS) with spherical protein-rich domains (coacervates) embedded within a continuous protein poor phase. The coacervates can coalesce and deform under shear stress (Boire et al., 2019; Ivanov et al., 2019). Recently, protein condensation initiated by coacervation of proteins in cells has attracted much attention as it is related to the stability and function of membraneless organelles and associated with several protein aggregation diseases including neurodegenerative disorders such as Alzheimer's disease and amyotrophic lateral sclerosis (Mitrea et al., 2018; Mitrea & Kriwacki, 2016). Outside cells, simple coacervation of protein has found applications in microencapsulation for lipophilic compounds (Lazko, Popineau, & Legrand, 2004), novel adhesive production (Mohammadi, Beaune, Stokke, Timonen, & Linder, 2018) and delivery of bioactive proteins (Lim, Ping, & Miserez, 2018). Simple coacervation has been observed for plant proteins, including soy glycinin (Chen, Zhao,

Nicolai, & Chassenieux, 2017b), pea protein (Cochereau, Nicolai, Chassenieux, & Silva, 2019), broadbean protein (Popello, Suchkov, Grinberg, & Tolstoguzov, 1992), gliadin (Boire, Menut, Morel, & Sanchez, 2013), zein (Muthuselvi & Dhathathreyan, 2006) and kafirin (Oguntoyinbo, Taylor, & Taylor, 2018). However, compared to the complex coacervation that usually occurs between oppositely charged proteins and polysaccharides (Schmitt & Turgeon, 2011), the investigation of the simple coacervation of protein is still quite limited.

Soy protein is widely used as an ingredient in the food industry for its good functional and nutritional properties. It contains two main components: glycinin and β-conglycinin with molar masses of about $3.6 \times 10^5$ and $2.0 \times 10^5$ g/mol, respectively (Nishinari, Fang, Guo, & Phillips, 2014). Soy glycinin has the lowest solubility at intermediate NaCl concentrations 0.1–0.2 M (Wolf, 1958). The solubility of glycinin is further decreased by lowering the temperature ( Lakemond, de Jongh, Hessing, Gruppen, & Voragen, 2000; Wolf & Sly, 1967). In a recent study, Chen et al. (2017b) show that the low solubility of glycinin at 0.1–0.2 M is related to the coacervation of glycinin. Initially, spherical protein rich domains are formed that with time coalesce into a continuous layer. Interestingly, β-conglycinin can partially inhibit the coacervation of soy glycinin (Chen et al., 2017b). Normally, depending on the type of the protein, the coacervates are destroyed upon the temperature change above or below a critical value and the turbid suspension becomes transparent at the same time (Raut & Kalonia, 2016). However, by heating glycinin coacervates, hollow protein microcapsules were formed (Chen et al., 2017b; Zhao, Guo, Ding, Ye, & Liu, 2019). Recently, similar phenomena have been reported also for pea protein (Cochereau et al., 2019). Further investigation showed that the soy glycinin microcapsules has pH and ionic strength responsive permeability (Chen, Zhang,

Mei, & Wang, 2018). Interestingly, in the presence of β-conglycinin with the glycinin/β-conglycinin ratio of 0.5–5, homogeneous microgels instead of hollow capsules are formed when the glycinin coacervates are heated (Chen et al., 2017b).

As mentioned above, in our previous work, we isolated the two components of soy protein, and mainly focused on the hollow microcapsules formed through the coacervation of glycinin under heating (Chen et al. 2017b; Chen et al. 2018). We also found that in the presence of a proper ratio of β-conglycinin, the coacervates could change into microgels instead of hollow microcapsules during heating (Chen et al., 2017b). However, the properties (e.g., swelling, loading capacity and mechanical properties) that relate to the application of these microgels are as yet unknown. Besides, the influence of the solvent conditions (salt concentration, pH, and temperature) on the glycinin coacervation in the presence β-conglycinin have not yet been investigated. SPI contains both glycinin and β-conglycinin at a ratio (1.27 – 3.6) that falls in the range (0.5–5) where microgels can be formed (Blazek, & Caldwell, 2009; Chen et al., 2017b). Therefore, the objective of the work presented here was to fabricate soy protein microgels by triggering the coacervation of glycinin in soy protein isolates (SPI) solutions and to investigate the properties of the microgels that are formed. We will first show the influence of the pH, the ionic strength, the protein concentration ($C$) and the temperature ($T$) on the coacervation of glycinin in SPI suspensions. Then we will demonstrate that SPI microgels can be fabricated by heating the SPI suspensions containing glycinin coacervates. The swelling behavior of the microgels upon changes in the pH or the ionic strength will be investigated. We will show that swollen microgels have a core-shell structure and discuss the possible formation mechanism of it. Finally, the interaction between the microgels and

macromolecules (dextran and lysozyme) was investigated in order to evaluate their potential as bioactive compound carriers. The current study is also different from our another previous work in which we focus on the nano-scale fractal aggregates and gel formation of SPI as influenced by salt. That work was conducted on homogenous SPI solutions in the presence of salt, but in the absence of coacervation (Chen, Zhao, Chassenieux, & Nicolai, 2017a).

## 2. Materials and Methods

### 2.1. Materials

Defatted soybean flour (7B) was kindly provided by Archer Daniels Midland Company, U.S. Rhodamine B and fluorescein isothiocyanate labeled dextran (FITC-dextran,150 kDa) were purchased from Sigma-Aldrich (St. Louis, MO. U.S.). FITC-lysozyme was purchased from Angfei Biotechnology Co., Ltd. (Guangzhou, China). Bicinchoninic acid (BCA) protein assay kits were purchased from Dingguo (Beijing, China). The water used in the research is deionized water. All other chemicals were of analytical reagent grade and obtained in China.

### 2.2. Soy protein isolate (SPI) preparation

SPI was prepared by dispersing the soybean flour in water at pH 7.5. The suspension was stirred at room temperature (23 ± 2 °C) for 1 h and then centrifuged at $10^4 g$ for 30 min. The supernatant was collected and centrifuged again at $10^4 g$ for 20 min after adjusting the pH to 4.5 to induce precipitation of the soy globulins. Deionised water was added to the collected precipitate at a ratio of 1:5 and the pH was adjusted to 7. The suspension was stirred until it became homogenous and centrifuged at $10^4 g$ for 30 min to remove insoluble material. The purified SPI solution was stored at 4 °C before use. The protein concentration was determined

using a BCA protein assay kit. SDS-PAGE showed that the purified SPI contained 64% glycinin and 32% β-conglycinin.

### 2.3. Preparation of protein solutions

SPI solutions with different concentrations were prepared from a stock solution at $C$ = 95 g/L and pH 6.7. The NaCl concentration of the protein solutions was set by adding aliquots of a concentrated NaCl solution (2 or 4 M) and the pH was set by adding 0.1 M HCl or NaOH. The SPI solutions were put in water baths at different temperatures to evaluate the influence of temperature on the coacervation. The turbidity and microstructure of the suspensions was probed with UV-visible spectrometry and confocal laser scanning microscopy (CLSM).

### 2.4. Fabrication of SPI microgels via coacervation

The pH of a SPI solution (20 g/L) was adjusted to pH 6.7. Then the ionic strength was adjusted to 0.1 M NaCl to induce coacervation and kept at 23 °C for 18 h while mildly stirring (200 rpm) during which the pH decreased to 6.25. Subsequently, the temperature of the suspension was increased to 80 °C, kept at 80 °C for 30 min in a water bath while stirring and then cooled back to room temperature. The microgels were isolated from the suspension by centrifugation at 5000*g* for 10 min and re-dispersed in water. The pH and ionic strength of the microgel suspension were adjusted by adding aliquots of 0.1 M NaOH, 0.1 M HCl or 2 M NaCl solutions to evaluate their swelling at different solvent conditions. The isolated microgels that dispersed in water were mixed with FITC-dextran (1 mg/mL) or FITC-lysozyme to investigate the diffusion of biomacromolecules into the microgels. The microstructure of each suspension was determined by CLSM.

## 2.5. Determination of the protein composition of the coacervates and the microgels

Microgel suspensions were centrifuged at 5000*g* for 10 min. The isolated microgels were solubilized by adding 1% sodium dodecyl sulfate (SDS). The protein concentration of the supernatant and the solubilized precipitate were determined using a BCA protein assay kit. The percentage of free protein released from the microgels was calculated by dividing the protein concentration in the supernatant by the total protein concentration. SDS-PAGE was used to determine the protein composition of the supernatant and the precipitate. The same procedure was used to determine the composition of the coacervate suspensions except that in this case the precipitates were solubilized in water.

## 2.6. Turbidity

The turbidity of the SPI solutions was determined by measuring the absorbance of the suspension at 500 nm using a UV-visible spectrometer E201 (Thermo Scientific, United States). Cuvettes with path lengths of 0.5 cm were used.

## 2.7. Confocal laser scanning microscopy (CLSM)

The soy proteins were physically labeled with the fluorochrome rhodamine B by adding a small amount of a concentrated rhodamine solution to the SPI suspensions to obtain a final concentration of 5 ppm. Samples were inserted between a concave slide and a coverslip. The microstructure of the suspensions at different solvent conditions were obtained at 20 °C with a Zeiss LSM 880 Confocal Microscope (Zeiss, Germany). A water immersion objective lens (63×/1.2NA) was used. The diffusion of FITC-dextran or FITC-lysozyme into the microgel was determined by measuring the fluorescence intensity of the FITC signal in the microgels.

The incident light was emitted by a laser beam at 561 nm for rhodamine B and at 488 nm for FITC. Transmitted light differential interference contrast (DIC) images were taken at the same time by the other channel. The particle size distribution (180 particles were counted) and fluorescence intensity profiles were obtained using the Image J software.

### 2.8. Zeta-potential and hydrodynamic diameter measurements

The surface charge of microgels at different pH or ionic strength and the diameter of the microgels dispersed in denaturing agents (dithiothreitol (DTT), urea or SDS) was determined by a commercial dynamic light scattering and microelectrophoresis device (Nano-ZS, Malvern Instruments, Worcestershire, UK). The device is equipped with a 633 nm laser and operates at a fixed angle of 173º. Notice that the value of the diameter is influenced by polydispersity and non-sphericity of the particles if they are larger than the inverse of the scattering wave vector, i.e. about 20 nm at 173°. This causes the measured apparent diameter to be less than the true z-average diameter.

### 2.9. Electrophoresis

Reducing sodium dodecyl sulfate-polyacrylamide gel electrophoresis (SDS-PAGE) was performed on a discontinuous buffered system, using 12% separating gel and 5% stacking gel. The protein sample was mixed with an equal volume of 2× reducing sample buffer which contained β-mercaptoethanol and then heated at 90 °C for 10 min. After the electrophoresis, the gel was stained using the Coomassie brilliant blue R-250 stain solution for 1 h and then soaked in de-staining solution (methanol/acetic acid/water, 1:1:8, v/v/v) for 24 h with two or

three changes of solution. The protein composition was analyzed by measuring the relative brightness of the bands using the Image J software.

## 3. Results and Discussion

### 3.1. Influence of adding NaCl on coacervation of glycinin in SPI solution

The ionic strength of SPI solutions at $C$ = 10 g/L and pH 7.0 was adjusted by adding 2 or 4 M NaCl. After 1 h of preparation, solutions at 0.1, 0.15 and 0.2 M NaCl became turbid, while at 0.05 and 0.5 M, the solutions remained clear (**Figure 1A**). The microstructure of the solutions was probed with CLSM (**Figure 1B**) which showed that after 1 h, SPI phase separated on microscopic length scales leading to the formation of well-defined spherical dense protein domains with diameters of approximately 1 μm. After 24 h, phase separation also occurred at 0.05 M, but it was less important than at 0.1 M. Clusters of domains appeared at 0.2 M. The suspensions containing 0.1 M NaCl were centrifuged after standing for 24 h and the precipitates were collected. The protein composition of the precipitates was analyzed by SDS-PAGE and compared with that of the SPI solution without phase separation. It showed that the proteins in the homogeneous SPI solution (lane 1) were composed of 64% glycinin and 32% β-conglycinin, whereas the precipitate from the phase separated SPI suspension (lane 2) contained 87% glycinin and 11% β-conglycinin (**Figure 1C**).

These observations show that simple coacervation of protein occurred in SPI solutions by adding salt which was caused by the association of glycinin. The low solubility of SPI at 0.1–0.2 M NaCl caused by association of glycinin has been reported before, but was not related to coacervation ( Wolf, 1958). Adding salt screened the electrostatic repulsion between protein

molecules (**Figure S1**) which promotes aggregation of the proteins, but it fails to explain why the solubility increased after adding more than 0.15 M NaCl even though the surface charge remained low. Jiang et al. (2015) has investigated in detail the influence of salt on the protein hydrophobicity and structure of SPI in aqueous solution. They showed that the solubility of SPI is negatively correlated with its hydrophobicity. The hydrophobicity was highest at 0.1 M NaCl which corresponded to the lowest solubility. In addition, at 0.1 M NaCl, the α-helix content in both SPI and glycinin solutions was lowest (Jiang, et al., 2015; Kim, Kim, Yang, & Kwon, 2004). Lakemond et al. (2000) have shown that the salt concentration influences the relative exposure of basic and acidic polypeptides of glycinin. As the basic polypeptide is more hydrophobic than the acidic one, the change of exposure will influence the surface hydrophobicity of the proteins. The present results show that the insolubility is in fact caused by coacervation which was reversible as the sediments obtained by centrifugation could be completely solubilized in water.

### 3.2. Influence of the pH on coacervation of glycinin in SPI solutions

The effect of the pH on coacervation of glycinin in SPI solutions in the presence of 0.1 M NaCl is shown in **Figure 2**. The pH was adjusted before adding salt. In salt free solutions, the solution remained homogeneous on microscopic length scales above pH 5.8, but irregular large flocs were observed below pH 5.8 (Chen et al., 2017b). After adding salt, see **Figure 2**, the solutions with an initial pH of 7.5 remained homogenous. However, for $6.6 \leq pH \leq 7.2$, well-defined spherical coacervates were observed. At pH 6.4, the coacervates tended to associate and finally at $pH \leq 6.2$, large irregular flocs were observed.

The protein coacervates dissolved when diluted in water, but the irregular flocs remained intact upon dilution. To form well defined spherical coacervates, molecular interaction must be large enough to drive association but not so large so as to avoid formation of strong bonds within and between coacervates (Amine, Boire, Kermarrec, & Renard, 2019; Comert & Dubin, 2017). The isoelectric point of glycinin is around pH 5. Decreasing the pH towards the isoelectric point reduces the charge density of the proteins, which decreases the strength of repulsive interactions between proteins and favors therefore their coacervation. However, at pH ≤ 6.4, the interaction became too strong, leading to flocculation.

### 3.3. Influence of the protein concentration on coacervation of glycinin in SPI solutions

The SPI stock solution ($C$ = 95 g/L, pH 6.7) was diluted to different protein concentrations followed by adjusting the NaCl concentration to 0.1 M. The microstructures of the suspensions (1 h and 24 h after preparation) are shown in **Figure 3A**. One hour after preparation, coacervation occurred at $C \leq 30$ g/L, but not yet at $C$ = 50 g/L. The size of the coacervates increased with increasing protein concentration. After one day, the coacervates had grown by coalescence and large coacervates had appeared also at $C$ = 50 g/L. No phase separation was observed for $C \geq 70$ g/L even after 3 days (**Figure S2**).

**Figure 3B** shows the evolution of the turbidity with time at 20 °C for SPI solutions at $C$ = 10, 20 and 50 g/L containing 0.1 M NaCl. The values were normalized by $C$ so as to correct for the trivial concentration dependence of the turbidity. For $C$ = 10 g/L, the turbidity increased weakly at first followed by a strong increase after about 20 min. At $C$ = 20 g/L, the turbidity remained low during 20 min and then increased more weakly than at $C$ =10 g/L. At $C$ = 50 g/L,

the turbidity remained low up to at least 120 min. These results confirm that the rate of glycinin coacervation decreases with increasing SPI concentration.

Above the denaturation temperature of the soy proteins, the inhibition effect of β-conglycinin on the glycinin aggregation by forming soluble complexes has been studied in detail in the past (Damodaran & Kinsella, 1982; Guo et al., 2012). In a recent study, it was found that at temperature as low as 20 °C and in the presence of β-conglycinin, the coacervation of glycinin was slowed down and the rate of coacervation decreased with increasing fraction of β-conglycinin (Chen et al., 2017b). This indicates that the inhibition effect of β-conglycinin exists even at low temperatures where the interactions between the two components are weaker and reversible (Chen et al., 2017b). For the SPI investigated here, the ratio of glycinin/β-conglycinin was fixed, and we found that by increasing the total protein concentration, the rate of coacervation decreased. We propose that two kinds of association may occur at the same time. One is the coacervation of glycinin triggered by adding salt and the other is the association between glycinin and β-conglycinin. At low protein concentrations, coacervation of glycinin is predominant, but with increasing protein concentration, the interaction between glycinin and β-conglycinin becomes more important, which decreases the tendency for glycinin to phase separate.

### 3.4. Influence of temperature on coacervation of glycinin in SPI solutions

The salt concentration of SPI solutions at $C$ = 20 g/L and pH 7.1 was adjusted to 0.1 M NaCl. At these conditions, no phase separation occurred just after adding salt. The solution was then immediately kept at different temperatures. **Figure 4A** shows the turbidity of SPI solutions

kept at different temperatures for 5 h. With increasing T, the turbidity decreased and reached a minimum at 40 °C. When *T* was further increased, the turbidity gradually increased again. The CLSM images show that only at $T < 40$ °C, spherical protein coacervates were observed (**Figure 4B**). Above 40 °C, no phase separation occurred and the visual appearance of the solution was semi-transparent (**Figure 4A**). These suspensions were then kept at room temperature (23 °C) for 18 h. The turbidity of the suspensions that were initially kept at 40–60 °C increased significantly compared to those before cooling (**Figure S3**) which was accompanied by the appearance of protein coacervates (**Figure 4B**). The solution that was initially kept at 80 °C still remained homogeneous without phase separation.

These results clearly show that two kinds of aggregation process occurred in the SPI solutions with increasing temperature, when 0.1 M NaCl was added, as accounted for by the presence of a characteristic temperature where the solutions showed lowest turbidity. At $T <$ 40 °C, coacervation of glycinin was predominant and was favored by lowering the temperature. At $T > 40$ °C, the coacervation was inhibited. Instead, thermal aggregation that leads to irreversible aggregation of SPI was gradually enhanced with increasing temperature. It has been shown previously that upon thermal denaturation in salt solutions, nanoparticles with radii less than 100 nm are formed at low protein concentrations which associate into large fractal aggregates at higher protein concentrations (Chen et al., 2017a). Furthermore, above a critical gel concentration, the aggregates percolate and form a gel (Chen et al., 2017a). The presence of protein coacervates after cooling was most likely due to the glycinin fraction that had not yet denatured during the thermal treatment. The denaturation extent increased with increasing temperature and was complete after keeping the sample at 80 °C for 5 h. Therefore, protein

302 coacervates were not formed in this case. The molecular interactions at play during thermal
303 aggregation have already been investigated in detail (Guo et al.,2012). It was shown that
304 hydrophobic interactions as well as disulfide bond formation are predominant, which makes
305 the structure of the aggregates formed upon heating stable and irreversible. The present results
306 show that, for protein coacervation, electrostatic interaction plays a more important role.
307 Furthermore, contrary to thermal aggregation, coacervation is reversible, i.e. the coacervates
308 can re-disperse when the solvent conditions are changed.

309 **3.5. Heat induced microgel formation from glycinin coacervates**

310 The pH of SPI solutions at 20 g/L was adjusted to pH 6.7 and the NaCl concentration of
311 the solutions was adjusted to 0.1 M. At these conditions, coacervation occurred immediately
312 after adding salt. The suspensions were kept stirring at 23 °C for 18 h in order to induce
313 formation of more protein coacervates and subsequently heated at 80 °C for 30 min to denature
314 the proteins. The microstructure of the suspensions as well as the particle size distribution and
315 the fluorescence intensity distribution of representative particles are shown in **Figure 5**. Before
316 heating, spherical protein coacervates with an average diameter of 1.9 μm were formed (**Figure**
317 **5A**). After heating, the coacervates transformed into microgels with a smaller average diameter
318 of approximately 1.4 μm (**Figure 5B**).

319 The microgels suspensions were centrifuged at 5000*g* for 10 min and the sedimented
320 microgels were re-dispersed in water. The pH of the microgel suspensions obtained in this
321 manner was 7. Interestingly, in water, the microgels swelled to a diameter of approximately
322 1.8 μm similar to that of the coacervates and showed a core-shell structure, which was attested

by the stronger fluorescence intensity at the edge, indicating a denser shell and a less dense core (**Figure 5C**). The thickness of the shell was approximatively 0.25 μm. By increasing the salt concentration back to 0.1 M NaCl, the microgels de-swelled and the core-shell structure disappeared (**Figure 5D**). The size of the microgels decreased back to around 1.3 μm.

The swelling and de-swelling behavior of the microgels could also be modulated by changing the pH (**Figure 6**). The microgels swelled with increasing pH to an average diameter of 2.3 μm at pH 10 and the shell thickness increased to 0.35 μm. When the pH was decreased to pH 6, the microgels de-swelled to an average diameter of 1.2 μm and the core shell structure was no longer visible. Below pH 6, i.e. closer to the isoelectric point, the microgels aggregated into clusters (**Figure S4**). However, when the pH was further decreased below 4, the microgels swelled again and the core-shell structure reappeared as shown in **Figure 6**. These results show that pH and ionic strength responsive core-shell SPI microgels were formed through protein coacervation. To our knowledge, fabricating protein microgels with a core-shell structure by protein self-assembly has not been reported before.

The pH and ionic strength responsive swelling and de-swelling behavior of the SPI microgels indicated that the electrostatic interaction plays an important role. The zeta-potential of the microgels suspension at different pH was measured (**Figure S5)**. Before adding salt, the pH of the suspensions was 7 and the microgels were negatively charged with a zeta-potential value of approximately -20 mV. Due to the strong electrostatic repulsion between the proteins, the microgels were swollen. When the NaCl concentration was increased to 0.1 M, the zeta-potential decreased to -9 mV. The decrease of electrostatic repulsion between the proteins

caused de-swelling of the microgels. With increasing pH above 7, the proteins carried more negative charges as shown by the increase of the zeta potential, which led to increasing electrostatic repulsion between the proteins. Therefore, the microgels swelled to a larger extent. Upon lowering pH towards the isoelectric point (pH 5.1), the net charge of the proteins decreased. Therefore, the electrostatic repulsion decreased, leading to de-swelling of the microgel between pH 4.5 and 6. When the pH was decreased below 4, the positive charge density of the proteins increased, causing an increase of the electrostatic repulsion and as a consequence swelling of the microgels. Swelling and de-swelling of protein microgels controlled by the charge density has earlier also been reported for whey protein microgels (Sağlam et al., 2013).

### 3.6. Protein composition of SPI microgels

The SPI microgel suspensions at different pH were centrifuged and the protein concentration in the supernatant was analyzed to determine the protein content that was released from the microgels (**Figure 7A**). The amount of protein that was released from the microgels was lowest (4%) between pH 4.5 and 6. With increasing pH above 6 or decreasing pH below 4.5, the released protein fraction increased to 56% at pH 3 and 10. At pH 11, the release of protein increased further to 68% and led to the partial dissociation of the microgels (**Figure S4)**. The protein composition of the supernatant and precipitates was analyzed by SDS-PAGE (**Figure 7B**). Between pH 6 and 4.5, the protein content in the supernatant was too low for a proper characterization of the composition. Below pH 4.5 or above 6, the main protein component in the supernatant was glycinin with only small amounts of β-conglycinin. This

means that some free glycinin that was not incorporated into the network of the microgels was released when they swelled. At pH 11, the microgels were partially dissociated (**Figure S4)** and more β-conglycinin was present in the supernatant compared to other pH values, indicating that β-conglycinin had been incorporated into the network of the microgel. SDS-PAGE analysis of the precipitates is shown in **Figure 7B** and the corresponding protein fractions are plotted as a function of the pH in **Figure S6**. Between pH 6.5 and 4.5, the main protein component of the precipitate was glycinin, which accounted for around 78% of the total amount of protein in the precipitate. With increasing pH above 6.5 or decreasing pH below 4.5, the amount of glycinin in the precipitate decreased to 49% at pH 3 and to 54% at pH 10 while the β-conglycinin content increased from 15% to 35% and 31%, respectively. This corroborates the findings that during swelling, free glycinin has been released from the microgels. Furthermore, SDS-PAGE analysis of the precipitates confirmed that both glycinin and β-conglycinin were incorporated into the network of the microgel. However, before heating, the main component of the coacervates was glycinin which accounted for 87% of the total protein in the precipitate (**Figure 1C**). With decreasing pH below 4 or increasing pH above 6.5, the content of basic polypeptide increased and became higher than that of the acid polypeptide, while between pH 4 and 6.5, the amount of the acid polypeptide was larger than that of the basic polypeptide (**Figure S6**). This indicates that more acid polypeptides were free and released from the microgels during swelling, whereas more basic polypeptides were bound to the microgels. Recently, Wu et al. have done a systematic investigation of the release of protein from SPI bulk gels (Wu, Hua, Chen, Kong, & Zhang, 2015; Wu et al., 2018). They found that the released proteins are mainly glycinin subunits and free acidic polypeptides while most of

β-conglycinin remains bound to the gel network, which is in accordance with our present results. One possibility to explain this behavior is the different denaturation temperature of the different subunits in glycinin, causing part of the glycinin to be not yet fully denatured and available to bind to the microgel network (Prak et al., 2005).

In the absence of β-conglycinin, glycinin coacervates transformed into hollow microcapsules (Chen et al., 2017b). Some free glycinin remained in the cavity of the microcapsules, but no network was formed in the cavity (Chen et al., 2018; Chen et al., 2017b). However, in the presence of β-conglycinin, a network was formed in the core of glycinin coacervate. We suggest that during heating β-conglycinin diffused into the coacervates and interacted with the glycinin which induced formation of a network in the core. This suggestion is supported by the finding that β-conglycinin has a tendency to interact with glycinin during heating (Damodaran & Kinsella, 1982; Guo et al., 2012).

In order to determine the interactions that stabilized the microgels, the microgel suspensions were adjusted to pH 8.5 and then centrifuged to remove free protein. The precipitates were subsequently dispersed in different solvents and the apparent hydrodynamic diameter was measured (**Figure 7C**). After addition of 40 mM DTT, 6 M urea or 1% SDS, the size of the microgels decreased, especially for those dispersed in 1% SDS. The size of the microgels further decreased by adding 40 mM DTT in addition to SDS or Urea. DTT can break disulfide bonds, while urea and SDS disrupt hydrophobic interactions. These results show that hydrophobic interactions are important to stabilize the microgel, but that disulfides bonds are also formed.

### 3.7. Influence of the pH on the diffusion of macromolecules into SPI microgels

Microgels have been widely applied as bioactive compound carriers (Bysell et al., 2011). By swelling or de-swelling the microgels, diffusion of molecules into or out of the microgels could be controlled. Here, FITC-dextran (150 kDa) was used as model bioactive compounds to check the diffusion of molecules into the microgels as a function of the pH (**Figure 8**). At pH 6.5, the dextran was excluded from the microgels resulting in low fluorescence intensity of the microgels. When the pH was 3.5, the dextran concentration in the microgels was higher than that in the bulk, causing stronger fluorescence by the microgels. At pH 10 and 3, the fluorescence intensity of the core of the microgel was almost the same as that of the bulk. However, at pH 3, the shell of the microgels showed stronger fluorescence while at pH 10 the fluorescence was less. The implication is that at pH 3 the dextran chains preferred to locate in the shell, whereas at pH 10 they were expelled from it.

The diffusion of molecules into the microgels depends on many factors, including the pore size of the network and the interaction with proteins. At pH 6.5, microgels display a net negative charge and FITC-dextran is also slightly negatively charged (Berth, Voigt, Dautzenberg, Donath, & Möhwald, 2002). Electrostatic repulsion could therefore be a reason for FITC-dextran to be excluded at pH 6.5. However, this does not explain the fluorescence of the cores at pH 10. It is also possible that the FITC-dextran chains were larger than the pores of the microgel at pH 6.5 and therefore could not easily penetrate into the microgels. The increase of the fluorescence intensity of the microgels with increasing pH would in that case be caused by an increase of the pore size caused by swelling. Another possible reason for the

429 penetration of dextran into the core at pH 10 is that at high pH, the structure of the protein
430 network is destabilized due to the cleavage of disulfide bonds and changes the protein structure
431 (Jiang, Xiong, Chen, 2011). At pH 3.5, the microgels were positively charged and swollen.
432 Due to the increased pore size of the network and the electrostatic attraction, the FITC-dextran
433 could penetrate and preferentially bind to the microgels. When the pH was readjusted back to
434 7, most of the FITC-dextran was released from the microgel (**Figure S7**). The decrease of the
435 contrast of the microgels at pH 3 compared to that at pH 3.5 was perhaps due to the increased
436 ionic strength caused by addition of more HCl. The fact that the diffusion of the molecules
437 could be controlled by the pH shows that the SPI microgels have the potential to be used as
438 bioactive compound carriers. Especially, electrostatic attraction between microgels and
439 molecules of opposite charges enhances the loading, which can be an efficient method for
440 encapsulating bioactive compounds such as proteins (Bysell et al., 2011). In the following
441 section, the interaction between microgels and oppositely charged proteins will be investigated.

442 **3.8. Binding and release of lysozyme to SPI microgels**

443 The microgel suspensions were incubated with lysozyme labeled with FITC at pH 9.
444 CLSM images of the mixtures are shown in **Figure 9A**. At low lysozyme concentrations, the
445 microgels showed a core-shell structure with stronger fluorescence displayed by the shell, i.e.
446 the shell contained a higher lysozyme content than the core. With increasing lysozyme
447 concentration, the fluorescence of the core increased while the microgels de-swelled slightly
448 and finally aggregated into clusters. At all concentrations, the microgels fluoresced strongly
449 implying binding of the lysozyme. Lysozyme, with an isoelectric point of pH 10.8, is positively

charged at pH 9 (Yi et al., 2017). It binds to the microgels that are negatively charged at pH > 5.1 due to the electrostatic attraction. With increasing lysozyme concentration, the amount of lysozyme that bound to the microgels increased which reduced the negative charge density of the microgels, leading to decreased electrostatic repulsion between proteins. Therefore, the microgels slightly de-swelled and finally aggregated into clusters.

The electrostatic attraction between lysozyme and the microgels can be reduced by adding salt or adjusting the pH to trigger the release of the lysozyme. **Figure 9B** shows the DIC and fluorescence images as well as merged images of the two channels for the lysozyme loaded microgel suspensions at different ionic strength. Profiles of the fluorescence intensity of representative microgels are also shown. With increasing NaCl concentration, the fluorescence intensity from FITC-lysozyme decreased implying that lysozyme was released. When the ionic strength was increased to 0.5 M, most of the lysozyme was released. The DIC images showed that the microgels remained intact in all cases. Salt screens the electrostatic attraction between the positively charged lysozyme and the negatively charged microgels, which explains why more lysozyme is released with increasing salt concentration. Release of the lysozyme also occurred after decreasing the pH to 3.5 (**Figure S8**), because the microgels became positively charged, causing electrostatic repulsion between microgels and lysozyme.

## 4. Conclusions

In summary, coacervation of glycinin in SPI solutions was influenced by the ionic strength, pH, protein concentration and temperature. It was promoted by increasing the NaCl concentration towards 0.1 M, decreasing the pH and lowering the temperature. Increasing the protein concentration slowed down the glycinin coacervation. Two types of self-assembly

processes were observed as a function of the temperature. Below about 40 °C, coacervation of glycinin was dominant and favored by decreasing temperature. Above 40 °C, thermal aggregation was dominant and favored by increasing temperature, with both glycinin and β-conglycinin participating. Heating the SPI suspensions containing glycinin coacervates led to formation of stable microgels with a core-shell structures, which were composed of both glycinin and β-conglycinin. The swelling and de-swelling of the microgels could be modulated by changing the electrostatic interaction. The microgels can be loaded with oppositely charged lysozymes and their release can be triggered by reducing the electrostatic interaction either by adding salt or by changing the pH. This demonstrates that SPI microgels can be used as bioactive compound carriers. Further research is needed to reveal the exact interaction between glycinin coacervates and β-conglycinin and the influence of solvent conditions on the microgel structure and their properties.

**Supplementary material**

Zeta-potential measurement of SPI solution in different NaCl concentration; Visual appearance of the 70g/L protein solution with 0.1 M salt at different times; Visual appearance of the SPI solution incubated at 40 and 60 °C with cooling to 23 °C; CLSM images of microgel suspension at pH 5 and pH 11; zeta-potential measurement of the microgel suspension; CLSM image of the microgel and FITC-dextran mixture under acidic condition with subsequent neutralization; images of SPI microgels loaded with lysozyme at basic conditions with subsequent adjustment of pH to 3.5.

**Funding sources**

This study was financially supported by Postdoctoral Innovation Talent Support Program, China (BX20190145), China Postdoctoral Science Foundation (2019M663387) and Natural Science Foundation of Guangdong Province, China (2019A1515011176).

**References**

Alves, A. C., & Tavares, G. M. (2019). Mixing animal and plant proteins: Is this a way to improve protein techno-functionalities? *Food Hydrocolloids, 97,*105171.

Amine, C., Boire, A., Kermarrec, A., & Renard, D. (2019). Associative properties of rapeseed napin and pectin: Competition between liquid-liquid and liquid-solid phase separation. *Food Hydrocolloids, 92,* 94–103.

Aymard, P., Williams, M. A. K., Clark, A. H., & Norton, I. T. (2000). A turbidimetric study of phase separating biopolymer mixtures during thermal ramping. *Langmuir, 16*, 7383-7391.

Berth, G., Voigt, A., Dautzenberg, H., Donath, E., & Möhwald, H. (2002). Polyelectrolyte complexes and layer-by-layer capsules from chitosan/chitosan sulfate. *Biomacromolecules, 3*, 579−590.

*Blazek, V., & Caldwell, R.A. (2009).* Comparison of SDS gel capillary electrophoresis with microfluidic lab-on-a-chip technology to quantify relative amounts of 7S and 11S proteins from 20 soybean cultivars. *International journal of food science and technology, 44*, 2127–2134.

Boire, A., Menut, P., Morel, M.-H., & Sanchez, C. (2013). Phase behaviour of a wheat protein isolate. *Soft Matter, 9*, 11417–11426.

514 Boire, A., Renard, D., Bouchoux, A., Pezennec, S., Croguennec, T., Lechevalier, V., Le Floch-
515 Fouéré, C., Bouhallab, S., & Menut, P. (2019). Soft-matter approaches for controlling
516 food protein interactions and assembly. *Annual Review of Food Science and*
517 *Technology, 10*, 521-539.
518 Bysell, H., Mansson, R., Hansson, P., & Malmsten, M. (2011). Microgels and microcapsules
519 in peptide and protein drug delivery. *Advanced Drug Delivery Reviews, 63*, 1172-1185.
520 Chen, L., Remondetto, G. E., & Subirade, M. (2006). Food protein-based materials as
521 nutraceutical delivery systems. *Trends in Food Science & Technology, 17*, 272-283.
522 Chen, N., Zhang, J., Mei, L., & Wang, Q. (2018). Ionic strength and pH responsive
523 permeability of soy glycinin microcapsules. *Langmuir, 34*, 9711-9718.
524 Chen, N., Zhao, M., Chassenieux, C., & Nicolai, T. (2017a). The effect of adding NaCl on
525 thermal aggregation and gelation of soy protein isolate. *Food Hydrocolloids, 70*, 88-95.
526 Chen, N., Zhao, M., Nicolai, T., & Chassenieux, C. (2017b). Exploiting salt induced
527 microphase separation to form soy protein microcapsules or microgels in aqueous
528 solution. *Biomacromolecules, 18*, 2064-2072.
529 Cochereau, R., Nicolai，Taco, Chassenieux, C., & Silva, J.V.C (2019). Mechanism of the
530 spontaneous formation of plant protein microcapsules in aqueous solution. *Colloids and*
531 *Surfaces A, 562*，213–219.
532 Comert, F., & Dubin, P. L. (2017). Liquid-liquid and liquid-solid phase separation in protein-
533 polyelectrolyte systems. *Advances in Colloid and Interface Science, 239*, 213-217.
534 Damodaran, S., & Kinsella, J. E. (1982). Effect of conglycinin on the thermal aggregation of
535 glycinin. *Journal of Agricultural and Food Chemistry, 30*, 812-817.

536 Dickinson, E. (2015). Microgels — An alternative colloidal ingredient for stabilization of food
537 emulsions. *Trends in Food Science & Technology, 43*, 178-188.
538 Guo, J., Yang, X. Q., He, X. T., Wu, N. N., Wang, J. M., Gu, W., & Zhang, Y. Y. (2012).
539 Limited aggregation behavior of b-conglycinin and its terminating effect on glycinin
540 aggregation during heating at pH 7.0. *Journal of Agricultural and Food Chemistry, 60,*
541 3782-3791.
542 Inthavong, W., Chassenieux, C., & Nicolai, T. (2019). Viscosity of mixtures of protein
543 aggregates with different sizes and morphologies. *Soft Matter, 15*, 4682-4688.
544 Ivanov, I., Lira, R. B., Tang, T. Y. D., Franzmann, T., Klosin, A., da Silva, L. C., Hyman, A.,
545 Landfester, K., Lipowsky, R., Sundmacher, K., & Dimova, R. (2019). Directed growth
546 of biomimetic microcompartments. *Advanced Biosystems, 3*, 1800314.
547 Jiang, J., Xiong, Y. L., & Chen, J. (2011). Role of β-conglycinin and glycinin subunits in the
548 pH-shifting-induced structural and physicochemical changes of soy protein isolate.
549 *Journal of Food Science, 76*, C293−C302.
550 Jiang, L., Wang, Z., Li, Y., Meng, X., Sui, X., Qi, B., & Zhou, L. (2015). Relationship between
551 surface hydrophobicity and structure of soy protein isolate subjected to different ionic
552 strength. *International Journal of Food Properties, 18*, 1059-1074.
553 Jiao, B., Shi, A., Wang, Q., & Binks, B. P. (2018). High-internal-phase pickering emulsions
554 stabilized solely by peanut-protein-isolate microgel particles with multiple potential
555 applications. *Angewandte Chemie International Edition in English, 57*, 9274-9278.

556 Kim, K. S., Kim, S., Yang, H. J., & Kwon, D. Y. (2004). Changes of glycinin conformation
557 due to pH, heat and salt determined by differential scanning calorimetry and circular
558 dichroism. *International Journal of Food Science and Technology, 39*, 385-393.
559 Lakemond, C. M. M., de Jongh, H. H. J., Hessing, M., Gruppen, H., & Voragen, A. G. J. (2000).
560 Soy Glycinin: Influence of pH and ionic strength on solubility and molecular structure
561 at ambient temperatures. *Journal of Agricultural and Food Chemistry, 48*, 1985-1990.
562 Lazko, J., Popineau, Y., & Legrand, J. (2004). Soy glycinin microcapsules by simple
563 coacervation method. *Colloids and Surfaces B: Biointerfaces, 37*, 1-8.
564 Lim, Z. W., Ping, Y., & Miserez, A. (2018). Glucose-responsive peptide coacervates with high
565 encapsulation efficiency for controlled release of insulin. *Bioconjugate Chemistry, 29*,
566 2176-2180.
567 Mitrea, D. M., Cika, J. A., Stanley, C. B., Nourse, A., Onuchic, P. L., Banerjee, P. R., Phillips,
568 A. H., Park, C. G., Deniz, A. A., & Kriwacki, R. W. (2018). Self-interaction of NPM1
569 modulates multiple mechanisms of liquid-liquid phase separation. *Nature*
570 *Communications, 9*, 842.
571 Mitrea, D. M., & Kriwacki, R. W. (2016). Phase separation in biology; functional organization
572 of a higher order. *Cell Communication and Signaling, 14*, 1.
573 Mohammadi, P., Beaune, G., Stokke, B. T., Timonen, J. V. I., & Linder, M. B. (2018). Self-
574 coacervation of a silk-Like protein and its use as an adhesive for cellulosic materials.
575 *ACS Macro Letters, 7*, 1120-1125.

576 Molliex, A., Temirov, J., Lee, J., Coughlin, M., Kanagaraj, A. P., Kim, H. J., Mittag, T., &
577 Taylor, J. P. (2015). Phase separation by low complexity domains promotes stress
578 granule assembly and drives pathological fibrillization. *Cell, 163*, 123-133.
579 Murray, B. S., & Phisarnchananan, N. (2016). Whey protein microgel particles as stabilizers
580 of waxy corn starch + locust bean gum water-in-water emulsions. *Food Hydrocolloids,*
581 *56*, 161-169.
582 Muthuselvi, L., & Dhathathreyan, A. (2006). Simple coacervates of zein to encapsulate Gitoxin.
583 *Colloids and Surfaces B: Biointerfaces, 51*, 39-43.
584 Nishinari, K., Fang, Y., Guo, S., & Phillips, G. O. (2014). Soy proteins: A review on
585 composition, aggregation and emulsification. *Food Hydrocolloids, 39*, 301-318.
586 Oguntoyinbo, S. I., Taylor, J. R. N., & Taylor, J. (2018). Comparative functional properties of
587 kafirin and zein viscoelastic masses formed by simple coacervation at different acetic
588 acid and protein concentrations. *Journal of Cereal Science, 83*, 16-24.
589 Phan-Xuan, T., Durand, D., Nicolai, T., Donato, L., Schmitt, C., & Bovetto, L. (2014). Heat
590 induced formation of beta-lactoglobulin microgels driven by addition of calcium ions.
591 *Food Hydrocolloids, 34*, 227-235.
592 Plamper, F. A., & Richtering, W. (2017). Functional microgels and microgel systems. *Accounts*
593 *of Chemical Research, 50*, 131-140.
594 Popello, I. A., Suchkov, V. V., Grinberg, V. Y., & Tolstoguzov, V. B. (1992). Effects of pH
595 upon the liquid-liquid phase equilibria in solutions of legumins and vicilins from broad
596 beans and peas. *Food Hydrocolloids, 6*, 147-152.

Prak, K., Nakatani, K., Katsube-Tanaka, T., Adachi, M., Maruyama, N., & Utsumi, S. (2005). Structure−function relationships of soybean proglycinins at subunit levels. *Journal of Agricultural and Food Chemistry, 53*, 3650−3657.

Raut, A. S., & Kalonia, D. S. (2016). Pharmaceutical perspective on opalescence and liquid−liquid phase separation in protein solutions. *Molecular Pharmaceutics, 13*, 1431−1444.

Sağlam, D., Venema, P., de Vries, R., Sagis, L. M. C., & van der Linden, E. (2011). Preparation of high protein micro-particles using two-step emulsification. *Food Hydrocolloids, 25*, 1139-1148.

Sağlam, D., Venema, P., de Vries, R., Shi, J., & van der Linden, E. (2013). Concentrated whey protein particle dispersions: Heat stability and rheological properties. *Food Hydrocolloids, 30*, 100-109.

Sağlam, D., Venema, P., de Vries, R., & van der Linden, E. (2013). The influence of pH and ionic strength on the swelling of dense protein particles. *Soft Matter, 9*, 4598–4606.

Schmitt, C., Moitzi, C., Bovay, C., Rouvet, M., Bovetto, L., Donato, L., Leser, M. E., Schurtenberger, P., & Stradner, A. (2010). Internal structure and colloidal behaviour of covalent whey protein microgels obtained by heat treatment. *Soft Matter, 6,* 4876–4884.

Schmitt, C., & Turgeon, S. L. (2011). Protein/polysaccharide complexes and coacervates in food systems. *Advances in Colloid and Interface Science, 167*, 63-70.

Wang, Y., Guo, L., Dong, S., Cui, J., & Hao, J. (2019). Microgels in biomaterials and nanomedicines. *Advances in Colloid and Interface Science, 266*, 1-20.

618 Wolf, W. J. (1958). Studies on the cold-insoluble fraction of the water extractable soybean
619 proteins. Factors influencing conformation changes in the 11S component. *Archives of*
620 *Biochemistry and Biophysics, 76*, 377-393.
621 Wolf, W. J., & Sly, D. A. (1967). Cryoprecipitation of soybean 11s protein. *Cereal Chemistry,*
622 *44*, 653–668.
623 Wu, C., Hua, Y., Chen, Y., Kong, X., & Zhang, C. (2015). Release behavior of non-network
624 proteins and its relationship to the structure of heat-induced soy protein gels. *Journal*
625 *of Agricultural and Food Chemistry, 63*, 4211-4219.
626 Wu, C., Navicha, W. B., Hua, Y., Chen, Y., Kong, X., & Zhang, C. (2018). Effects of removal
627 of non-network protein on the rheological properties of heat-induced soy protein gels.
628 *Lwt - Food Science and Technology, 95*, 193-199.
629 Yi, S., Dai, F., Ma, Y., Yan, T., Si, Y., & Sun, G. (2017). Ultrafine silk-derived nanofibrous
630 membranes exhibiting effective lysozyme adsorption. *ACS Sustainable Chemistry &*
631 *Engineering, 5*, 8777-8784.
632 Zhao, H., Guo, M., Ding, T., Ye, X., & Liu, D. (2019). Exploring the mechanism of hollow
633 microcapsule formation by self-assembly of soy 11s protein upon heating. *Food*
634 *Hydrocolloids,* https://doi.org/10.1016/j.foodhyd.2019.105379.

## Figure Captions

**Figure 1.**Visual appearance **(A)** and CLSM images **(B)** of SPI solutions (10 g/L, pH 7) at different NaCl concentrations. The images were taken 1 h (top row) and 24 h (bottom row) after adding salt. The scale bar represents 5 μm. **(C)** Protein composition of the SPI solution (lane 1) and the precipitates (lane 2).

**Figure 2.** CLSM images of SPI solutions ($C$ = 10g/L) adjusted to different pH and subsequently to [NaCl] = 0.1 M. Images were taken 2 h after preparation. The scale bar represents 5 μm.

**Figure 3. (A)** CLSM images of SPI solutions at different protein concentrations at 0.1 M NaCl. Images were taken after 1 h (top row) and 24 h (bottom row). The scale bar represents 5 μm. **(B)** Evolution of the turbidity with time at 20 °C for SPI solutions at different protein concentrations in the presence of 0.1 M NaCl.

**Figure 4. (A)** Turbidity of SPI suspensions (20 g/L, 0.1 M NaCl) kept at different temperatures for 5 h. The inserted picture shows the visual appearance of the suspensions. **(B)** CLSM images of SPI solutions incubated at different temperatures for 5 h (top row) and subsequently kept at 23 °C for 18 h (bottom row). The scale bar represents 10 μm.

**Figure 5.** CLSM images, particle size distributions and fluorescence intensity profiles of representative particles for a SPI suspension with glycinin coacervates **(A)**; a SPI suspension with glycinin coacervates after heating at 80 °C for 30 min **(B)**; microgels dispersed in water **(C)**; microgels dispersed in 0.1 M NaCl **(D)**. The scale bar represents 5 μm.

**Figure 6.** CLSM images, particle size distribution and fluorescence intensity profiles of representative particles of SPI microgels at different pH. The scale bar represents 5 μm.

**Figure 7. (A)** Percentage of protein released from the microgels. **(B)** SDS-PAGE slabs of the supernatant and precipitate of microgel suspensions at different pH. **(C)** Apparent hydrodynamic diameter of microgels dispersed in different denaturing agents: 40 mM DTT, 6 M Urea, 1% SDS, 6 M Urea + 40 mM DTT, 1% SDS + 40 mM DTT.

**Figure 8.** CLSM images of microgel suspensions in the presence of FITC-dextran at different pH. The scale bar represents 5 μm.

**Figure 9. (A)** CLSM images of suspensions of microgels with FITC-lysozyme at different concentrations indicated in the images. **(B)** DIC/Fluorescence CLSM images and profiles of the fluorescence intensity of microgels loaded with lysozyme dispersed in water with different NaCl concentrations. The scale bar represents 5 μm.

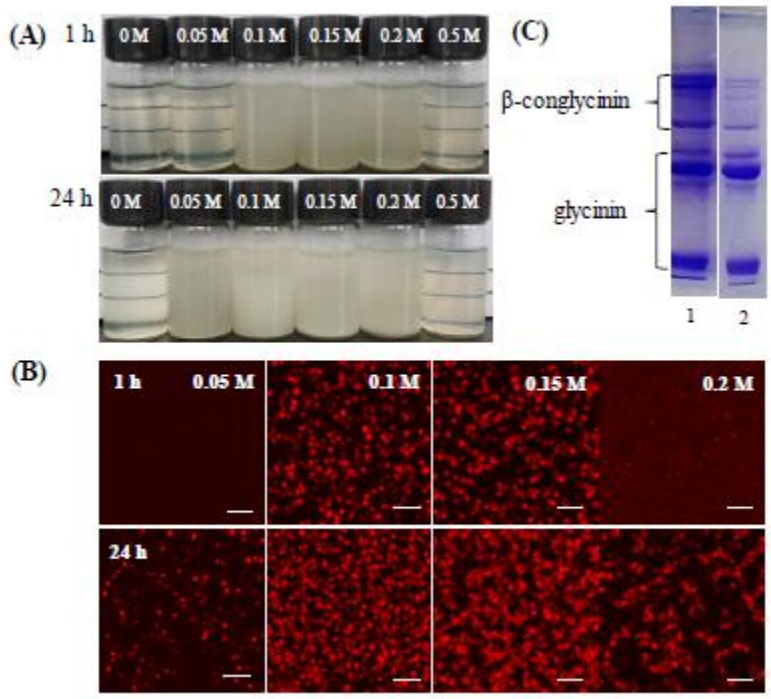
(A)
1 h
0 M
0.05 M
0.1 M
0.15 M
0.2 M
0.5 M
24 h
0 M
0.05 M
0.1 M
0.15 M
0.2 M
0.5 M
(C)
β-conglycinin
glycinin
1
2
(B)
1 h
0.05 M
0.1 M
0.15 M
0.2 M
24 h

Figure 1.

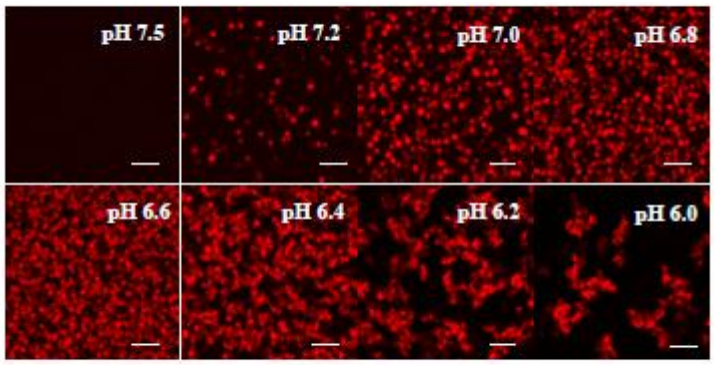


**Figure 2.**

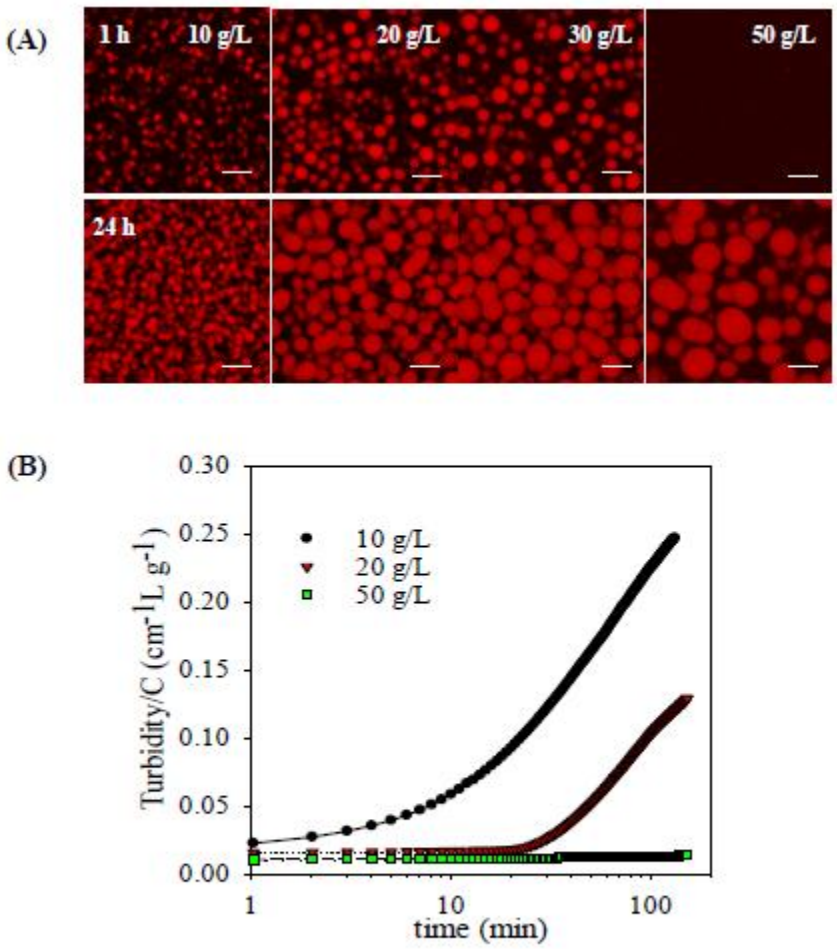
(A)
1 h
10 g/L
20 g/L
30 g/L
50 g/L
24 h
(B)
Turbidity/C (cm-1L g-1)
0.30
0.25
0.20
0.15
0.10
0.05
0.00
10 g/L
20 g/L
50 g/L
1
10
100
time (min)

**Figure 3.**

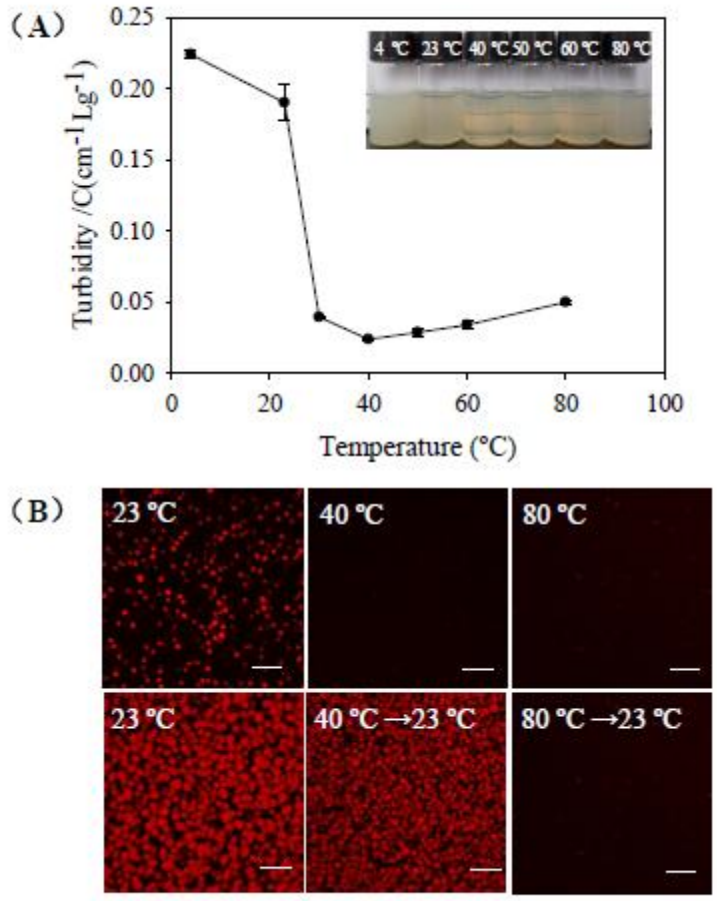
(A)
Turbidity /C(cm-1Lg-1)
0.25
0.20
0.15
0.10
0.05
0.00
0
20
40
60
80
100
Temperature (°C)
4 ℃ 23 ℃ 40 ℃ 50 ℃ 60 ℃ 80 ℃
(B)
23 ℃
40 ℃
80 ℃
23 ℃
40 ℃→23 ℃
80 ℃→23 ℃

**Figure 4.**

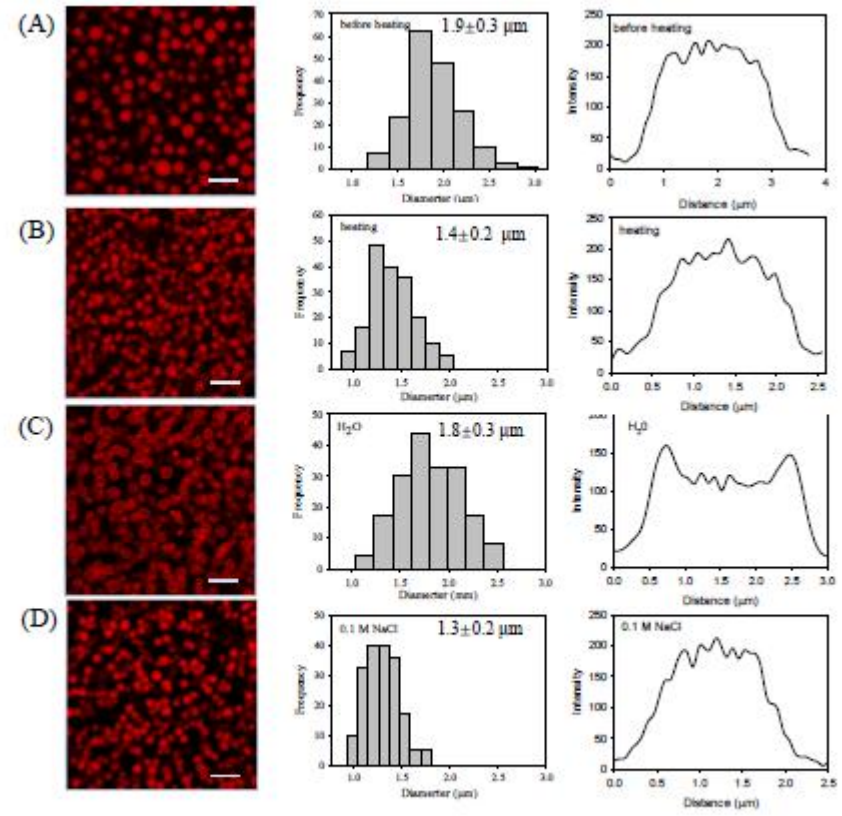
(A)
(B)
(C)
(D)
before heating
1.9±0.3 μm
heating
1.4±0.2 μm
H2O
1.8±0.3 μm
0.1 M NaCl
1.3±0.2 μm
Frequency
Diameter (μm)
Intensity
Distance (μm)

**Figure 5.**

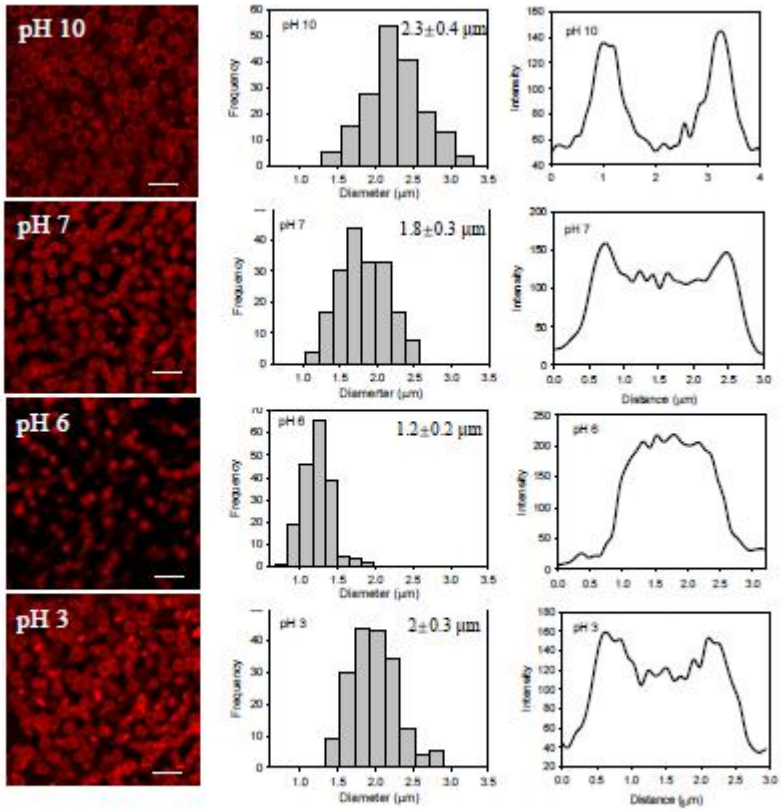
pH 10
pH 7
pH 6
pH 3
2.3±0.4 µm
1.8±0.3 µm
1.2±0.2 µm
2±0.3 µm
Frequency
Diameter (µm)
Intensity
Distance (µm)

**Figure 6.**

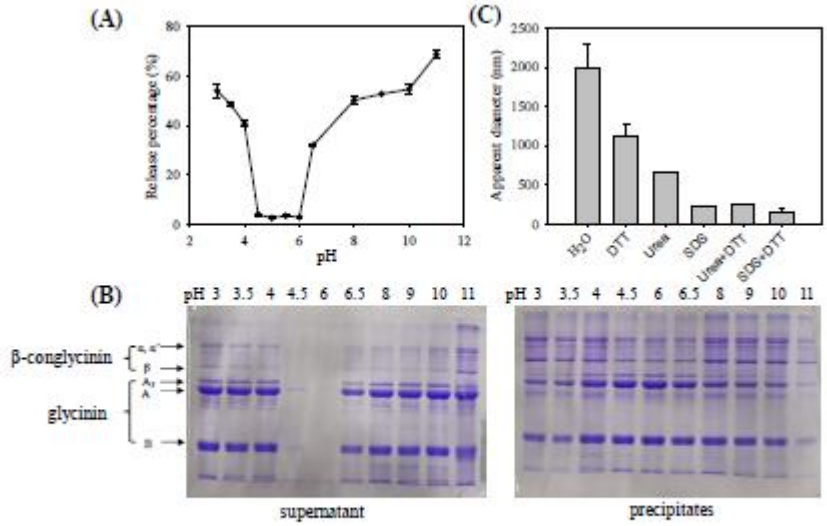
(A)
Release percentage (%)
pH
(C)
Apparent diameter (nm)
H2O
DTT
Urea
SDS
Urea+DTT
SDS+DTT
(B)
pH 3 3.5 4 4.5 6 6.5 8 9 10 11
β-conglycinin
glycinin
supernatant
precipitates

**Figure 7.**

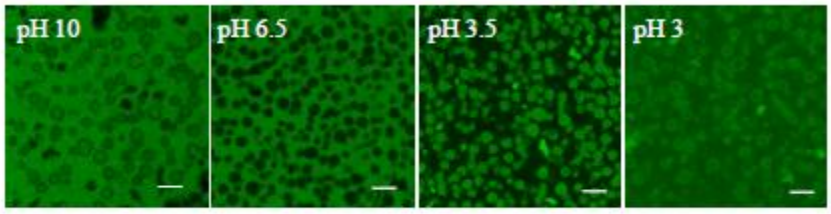


Figure 8.

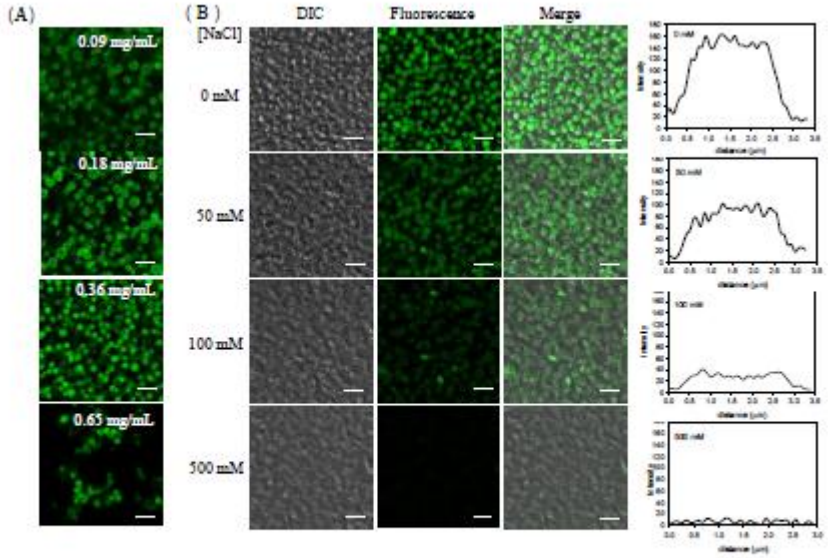


17

18 **Figure 9.**

687

688